Role of Side-chains in the Cooperative β-Hairpin Folding of the Short C−Terminal Fragment Derived from Streptococcal Protein G†

Naohiro Kobayashi, Shinya Honda,‡ Hirofumi Yoshii, and Eisuke Munekata*

Institute of Applied Biochemistry, University of Tsukuba, Tsukuba, Ibaraki 305-8572, Japan and National Institute of Bioscience and Human-Technology, Tsukuba, Ibaraki 305-8566, Japan

Received January 4, 2000; Revised Manuscript Received April 3, 2000

ABSTRACT: A short C-terminal fragment of immunoglobulin-binding domain of streptococcal protein G is known to form nativelike β-hairpin at physiological conditions. To understand the cooperative folding of the short peptide, eight Ala-substituted mutants of the fragment were investigated with respect to their structural stabilities by analyzing temperature dependence of NMR signals. On comparison of the obtained thermodynamic parameters, we found that the nonpolar residues Tyr45 and Phe52 and the polar residues Asp46 and Thr49 are crucial for the β-hairpin folding. The results suggest a strong interaction between the nonpolar side chains that participates in a putative hydrophobic cluster and that the polar side chains form a fairly rigid conformation around the loop (46−51). We also investigated the complex formation of the mutants with N-terminal fragment at the variety of temperature to get their thermal unfolding profiles and found that the mutations on the residues Asp46 and Thr49 largely destabilized the complexes, while substitution of Asp47 slightly stabilized the complex. From these results, we deduced that both the hydrophobic cluster formation and the rigidity of the loop (46−51) cooperatively stabilize the β-hairpin structure of the fragment. These interactions which form a stable β-hairpin may be the initial structural scaffold which is important in the early folding events of the whole domain.

Protein fragments are generally considered to be an ideal model for characterizing the denatured state of a protein in a physiological condition and allows one to focus on the native interactions in specific region of the protein. To understand the early events of protein folding, fragments of proteins have been analyzed by many spectroscopic approaches such as NMR[1] and CD (*1*−*12*). In these studies, some residual structures have been found in the fragments, which is clearly distinct from the peptide in a completely random-coiled state. Concerning these facts, there is much debate on various proposed models of protein folding, such as the framework model (*13*), the embryos model (*14*), the nucleation-condensation model (*15*), and the foldon model (*16*).

The immunoglobulin binding domain of protein G (*17*−*20*) reveals a peculiar folding topology as determined in solution (*21*, *22*) (Figure 1) and crystal (*23*, *24*). The thermodynamic and kinetic studies of the domain have been studied (*25*, *26*), and it was concluded that the domain folds/unfolds as a two-state transition without accumulating any equilibrium or kinetic intermediates. However, a recent study by ultrarapid mixing experiments (*27*) has successfully elucidated an intermediate state of Protein G and a sequential three-state mechanism was proposed. To elucidate the folding mechanism of the domain, we have investigated the conformational properties of the variable fragments derived from the protein G B1 domain by ^{1}H NMR and we have shown that a nonrandom coil structure exists in the C-terminal fragment (*28*), termed PGB1(41−56)[2] in this study. Afterward, Blanco et al. has demonstrated that the fragment forms

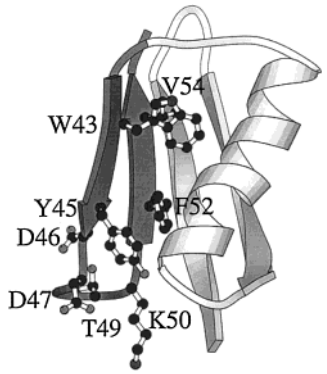

FIGURE 1: Ribbon model showing the conformation of the B1 domain of streptococcal protein G (*21*) drawn using the program MolScript (*44*). The C-terminal segment corresponding to PGB1-(41−56) is darkened. The side chains of the residues mutated in this study are represented with bolls and sticks.

† This work was supported by a research grant from a Grant-in Aid for Scientific Research from the Ministry of Education, Science and Culture of Japan (07406005) and a grant from the Ministry of International Trade and Industry of Japan.

* To whom correspondence should be addressed. Phone: +81-298-53-6625. Fax: +81-298-53-6277. E-mail: munekata@sakura.cc.tsukuba.ac.jp.

‡ National Institute of Bioscience and Human-Technology, Tsukuba 305, Japan.

[1] Abbreviations: PGB1(1−40), N-terminal fragment of the B1 domain from streptococcal protein G; PGB1(41−56), C-terminal fragment of the B1 domain from streptococcal protein G; Fmoc, 9-fluorenylmethoxycarbonyl; ^{t}Bu, *tert*-butyl; Trt, triphenylmethyl; Boc, *tert*-butyloxycarbonyl; DCC, 1,3-dicyclohexylcarbodiimide; HOBt, *N*-hydroxybenzotriazole; HBTU, 2-(1H-benzotriazole-1-yl)-1,1,3,3-tetramethyllironium hexafluorophosphate; HMP, 4-hydroxymethylphenoxy; TFA, trifluoroacetic acid; EDT, ethandithiol; HPLC, high-performance liquid chromatography; TSP, sodium-3-trimethylsilylpropionate-d_4; CD, circular dichroism; NMR, nuclear magnetic resonance.

10.1021/bi000013p CCC: $19.00
Published on Web 05/05/2000

a nativelike β-hairpin structure in aqueous solution (*29*). Recently, the equilibrium and kinetics studies on the β-hairpin folding using laser temperature jump experiments and statistical mechanical calculations showed that the peptide rapidly and cooperatively forms the secondary structure and that the folding can be depicted as a two-state folding process (*30*, *31*). The previous NMR study (*29*) and theoretical and computational studies (*31*−*33*) suggested that the hydrophobic interactions among the side chains of Trp43, Tyr45, Phe52, and Val54 mainly contribute to the β-hairpin folding; however, no experimental evidence of the side chain's roles has been reported yet.

The folding and unfolding rates of globular proteins are usually slower than the NMR time scale, thus the signals derived from native and denatured species in equilibrium state are observed as separate signals, and their intensities correspond to the folded and unfolded fractions, respectively (*34*). If, however, such folding rates were faster than the NMR time scale, then only one signal would appear, in which the chemical shifts of the signal would reflect the averaged value of folded and unfolded fractions (*35*). The ^{1}H chemical shifts are highly reproducible, and these values are independent of either sample concentration or inhomogenieties of magnetic field provided that the samples are at the same temperature and pH. This is because the chemical shift is highly sensitive to changes of the chemical environment around the proton of interest. Therefore, for the rapid folding and unfolding protein, it is possible to determine the folded and unfolded fractions from the change in chemical shift. Recently, we have developed a new analytical procedure using temperature dependence of chemical shifts to evaluate the thermodynamic stability of a short peptide (*36*). This method of analysis was applied to the study on PGB1(41−56). As a result, we have found that all the nonpolar side chain and α-proton signals of the PGB1(41−56) showed the same temperature dependence. The fact indicates high cooperativity of the hairpin folding occurring throughout the molecule, and this cooperativity has been further confirmed by calorimetric measurements. The chemical shifts of nonpolar side-chain signals were found to be more sensitive to temperature change than those of α-protons, so that these chemical shifts provide more accurate thermodynamic parameters, which can be used for quantitative examination of the stability of PGB1(41−56) mutants.

In previous papers, we have shown that the N-terminal fragment of protein G, PGB1(1−40), binds noncovalently to the PGB1(41−56), forming a complex with a nativelike conformation (*37*, *38*). Moreover, our recent study using a PGB1(41−56) mutant with a disulfide connecting its N- and C-terminus (*39*) has suggested that the stabilization of PGB1(41−56) could accelerate the folding process of the whole domain. Such stability of the PGB1(41−56) gives rise the possibility of an important role of β-hairpin formation, which reduces the entropic distribution of the C-terminal region in the early folding events of the domain. Therefore, the complex formation with PGB1(1−40) would be expected to be a good paradigm to study how the mutations on the PGB1(41−56) region of the domain would affect the thermodynamic stability or folding kinetics of the whole domain.

The side chains of Trp43, Tyr45, Phe52, and Val54 are buried in the hydrophobic core of the native domain, whereas Asp46, Asp47, Thr49, and Lys50 are solvent accessible and placed in the unique loop structure of the domain (see Figure 1). In this study, we have investigated the structural and thermodynamic nature of eight PGB1(41−56) mutants, in which Trp43, Tyr45, Asp46, Asp47, Thr49, Lys50, Phe52, and Val54 were substituted by alanine, to know not only the role of each side chain for stabilizing the β-hairpin but also whether there is a cooperative contribution among the polar and nonpolar side chains on the β-hairpin folding. Moreover, the complex formation of the PGB1(41−56) mutants with PGB1(1−40) was also investigated with respect to their thermodynamic stabilities. The determined thermodynamic parameters of the mutants alone and the complexes are compared with wild-type, and the implication of the β-hairpin formation in the folding process of protein G is discussed.

MATERIALS AND METHODS

Synthesis of Peptides. All peptides described in this report were synthesized using a conventional solid-phase method combined with a manual synthesis protocol that we have established (*33*, *35*). All amino acids were protected at the α-amino group with Fmoc group. The side chains of Asp, Glu, Thr, and Tyr were protected with ^{t}Bu-group, Asn, and Gln with Trt group, and Lys was protected with Boc group. Coupling reactions proceeded according to standard Fmoc strategy using DCC-HOBt and HBTU-HOBt methods on an HMP resin support. After elongation of the full length of the peptide, the resins were treated with 20% piperidine for 20 min, followed by TFA-H_2O-EDT (9.5:0.25:0.25) treatment for 1 h. The obtained crude peptides were purified by preparative reversed-phase HPLC using an Inertsil ODS column (25 × 250 mm). The homogeneity of the purified peptides was confirmed by analytical reversed-phase HPLC using a Wakosil 5C18 column (4.6 × 250 mm). The amino acid components were analyzed with a Hitachi L-8500 amino acid analyzer, the sequences with a Shimazu PPSQ-10 amino acid sequencer and the molecular mass with a JEOL JMS-HX110HF double-focusing mass spectrometer.

CD Spectrum Measurement. CD spectra of the PGB1(41−56) mutants were measured from 260 to 195 nm using a JASCO J-600 spectropolarimeter calibrated with (+)-10-camphorsulfonic acid. Lyophilized powdered peptides for CD spectra were dissolved in 5 mM phosphate buffer at pH 7.0, and the pH values were adjusted with 1 N HCl or NaOH.

Sample Preparation for NMR Spectroscopy. Samples for NMR measurements were prepared by dissolving the peptides in 99.996% D_2O. These solutions contained 5 mM sodium phosphate buffer and a small amount of TSP as a reference for zero ppm. The pH of the solutions was adjusted to an accuracy of ±0.02 by titration with HCl or NaOH using a glass microelectrode without correction for the isotope effect. The concentrations of the peptides were determined using the molar extinction coefficients for tryptophan and tyrosine in model compounds (*40*).

NMR Spectroscopy. NMR spectra were acquired with Bruker AMX500 or AM500 spectrometers. 1D ^{1}H NMR

[2] The primary sequence of PGB1(41−56) is GEWTYDDATKTFTVTE.

spectra were obtained by accumulating data from 32 to 256 scans and four preceding dummy scans into 8K data points for 1D and zero-filled into 32K data points.

The temperature dependence of NMR signals of the PGB1-(41−56) mutant alone was performed by measuring 1D ^{1}H NMR spectra increasing in the temperature from 278 to 358K at 5K intervals. Eurotherm temperature controlling system B-CU05 equipped on the Bruker AMX 500 NMR spectrometer, which provided a good feasibility (below ±0.01 K) on the temperature control for all experiments. The 1D data multiplied by a squared cosine-bell weighting function were zero-filled into 32K data points for 10 ppm of spectral width. Resultant resolution for chemical shift per data points were 0.625×10^{-3} ppm/points which were below the smallest chemical shift change of C$^{\delta}$H-Tyr45 resonance of the mutant D46A, 0.71×10^{-3} ppm/points between 333 and 338 K.

For analyzing the thermodynamic stability of the complexes of PGB1(41−56) wild-type and mutants with PGB1-(1−40), 1D ^{1}H NMR of the equimolar mixture (0.5 mM) of the peptides were measured from 276 to 333 K. To evaluate the fraction of bound state of PGB1(41−56) and mutants to PGB1(1−40), C$^{\zeta}$H-Phe52 and C$^{\gamma}$H$_3$−Val54 signals were integrated manually.

Thermodynamic Analysis for a Short Fragment. The data of the chemical shifts of several side chains versus temperature (chemical shift melting curve) were analyzed on the theory of a two-state phase transition as performed in our previous study on PGB1(41−56) wild-type (*36*) using a combination of the reciprocal temperature plot (RT plot) analysis and the restricted nonlinear fitting calculations. First, a rough estimation of the thermodynamic parameters of PGB1(41−56) mutants was carried out by the RT plot analysis. For a final refinement, it was followed by a restricted nonlinear fitting calculation using the parameter from the RT plot analysis as an initial condition. The following equation was used for the calculation:

$$Y = \frac{Y_U + (Y_F - Y_U)}{\left(\exp\left[-\frac{\Delta H_m}{R}\left(\frac{1}{T} - \frac{1}{T_m}\right)\right] + 1\right)} \quad (1)$$

where Y represents the observed chemical shift value of the proton signal at the varied temperatures, while Y_F and Y_U are the values in the completely folded and unfolded states of the mutants, respectively. ΔH_m is the enthalpy change upon unfolding at the transition temperature T_m. Y_F, Y_U, and ΔH were assumed constant at any temperatures. The heat capacity change was excluded in the calculation as the exposed hydrophobic surface area upon unfolding for a short peptide is expected to be negligible. Theoretically, the NMR signals of ideally unfolded proteins would depend on only local chemical environment, e.g., the primary sequence, not on the native tertiary structure. This allows reasonable fixing of Y_U values of all protons for each mutant to a corresponding value of the PGB1(41−56) wild-type. The inflection point obviously appeared in the RT plots of one mutant, revealing a wide coverage of the melting curves over a half of the transition. For this mutant, therefore, any further assumption was not applied for the refinement calculation of thermodynamic data, thus the value of Y_F was set to be variable. For the other mutants, Y_F was set to be equal to those of the wild-type as a first approximation. All computational calculations were carried out using SigmaPlot (SPSS Inc.) software.

Thermodynamic Analysis for a Complex. The data of the intensity of NMR signals versus temperature (intensity melting curve) were analyzed on the three component theory (AB ⇌ A + B) as described previously (*38*). Thermodynamic parameters, ΔH_m and T_m, were determined by solving the following equations numerically:

$$I = I_F(1 - f) = I_F\left(1 - \frac{-K + \sqrt{K^2 + 4C_tK}}{2C_t}\right) \quad (2)$$

$$K = \frac{C_t}{2}\exp\left\{-\frac{\Delta H_m}{RT}\left(1 - \frac{T}{T_m}\right) - \frac{\Delta C_p}{RT}\left[T - T_m - T\ln\left(\frac{T}{T_m}\right)\right]\right\} \quad (3)$$

where I represents the observed intensity of the proton signal at varied temperatures, while I_F the intensity in the completely folded state of the complex. I_F was assumed to be constant at any temperatures. f and K denote the molar fraction of the unfolded molecule and the equilibrium constant, respectively. C_t is the initial concentration of the fragments that were mixed at an equivalent molecular ratio, i.e., $C_t = A = B$. ΔH_m is the change in enthalpy upon unfolding at the transition temperature T_m. ΔC_p is the change in heat capacity upon unfolding, which was assumed to be constant at any temperatures and fixed at the value of the wild-type complex (2.6 kJ mol^{-1} K^{-1}) established in our previous study (*39*). All computational calculations were carried out using SigmaPlot (SPSS Inc.) software.

RESULTS

Solubility of PGB1(41−56) Mutants in Aqueous Solution. In aqueous solution, a short peptide with low solubility tends to form aggregates at millimolar concentrations, which would cause a significant line broadening on NMR spectra. It would be most likely to find the aggregation in a mutant that is substituted on hydrophilic amino acid with more hydrophobic one. The mutants W43A, Y45A, T49A, F52A, and V54A were easily dissolved in 5−50 mM sodium phosphate buffer at pH 5−7 and 276−298 K in a concentration range of 2−3 mM. No changes in their CD spectra (data not shown) were observed after storage on 277 K for 1 month. On the other hand, we found a less solubility of the mutants D46A, D47A, and K50A forming gel or precipitation in the solution at 1 mM peptide concentration. These mutants showed a negative peak at 230 nm in the CD spectra (data not shown), suggesting a formation of soluble aggregates including β-sheet structures (*41*, *42*). In this study, the concentration of these peptides was optimized by observing the line broadening in 1D ^{1}H NMR and the negative peak at 230 in CD spectra or the precipitation in the solution. After the optimization, all 1D ^{1}H NMR spectra of the mutants (showed in Figure 2) revealed fine line shapes at 298 K, indicative of no considerable aggregation in those samples.

Aromatic and Aliphatic Signals in PGB1(41−56) Mutants in Comparison with Wild-Type. First, we observed the aromatic and aliphatic NMR signals of eight PGB1(41−56)

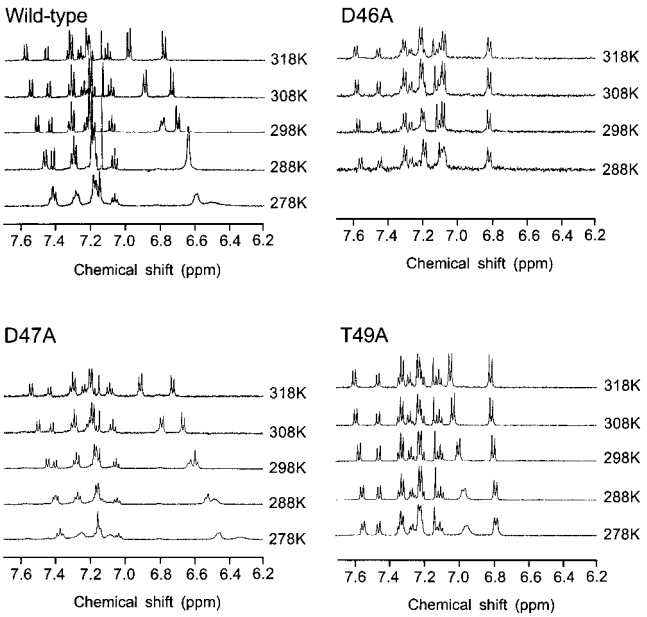

FIGURE 2: Aromatic region of 1D ^{1}H NMR spectra for some PGB1-(41−56) mutants measured at various temperatures. The peptide concentration was 0.2−1.0 mM in 5 mM sodium phosphate buffer at pH 7.0 in D_2O.

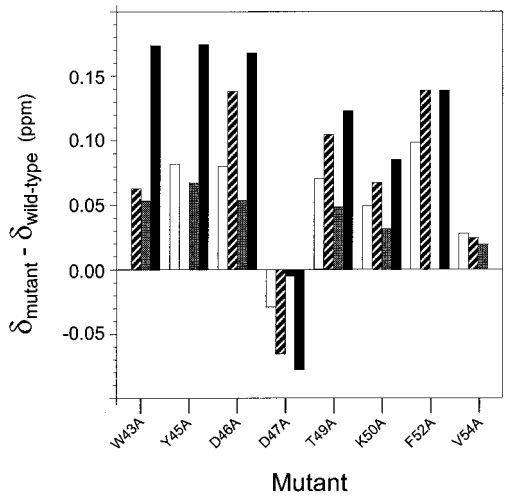

FIGURE 3: Chemical shift differences of aromatic signals between PGB1(41−56) and its mutants at 298 K. All values are indicated as an open bar; C$^\epsilon$H-Trp43, a hatched bar; C$^\epsilon$H-Tyr45, a shaded bar; C$^\zeta$H-Phe52 and a closed bar; C$^\gamma$H$_3$-Val54.

mutants. The mutants W43A, D47A, K50A, and V54A showed large chemical shift changes, while the chemical shift of the mutants Y45A, D46A, and F52A were obviously independent of the temperature range from 278 to 338 K. The chemical shift deviations between the wild-type and the mutants at 298 K are shown in Figure 3. For example, the mutation of Phe52 largely influenced the temperature dependencies on the signals C$^\epsilon$H-Trp43, C$^\delta$H-Tyr45, and C$^\gamma$H$_3$-Val54, whose residues are away from the substitution site. These facts clearly indicate that the influence of the mutations on Trp43, Tyr45, Asp46, and Phe52 are not localized on a certain region close to the mutation site but influences on the whole molecule.

Thermodynamic Analysis for PGB1(41−56) Mutants. In the 1D ^{1}H NMR spectra of wild-type, D47A and V54A, the temperature dependencies of the aromatic and aliphatic signals were remarkable, for example, C$^\delta$H-Tyr45, 15.0

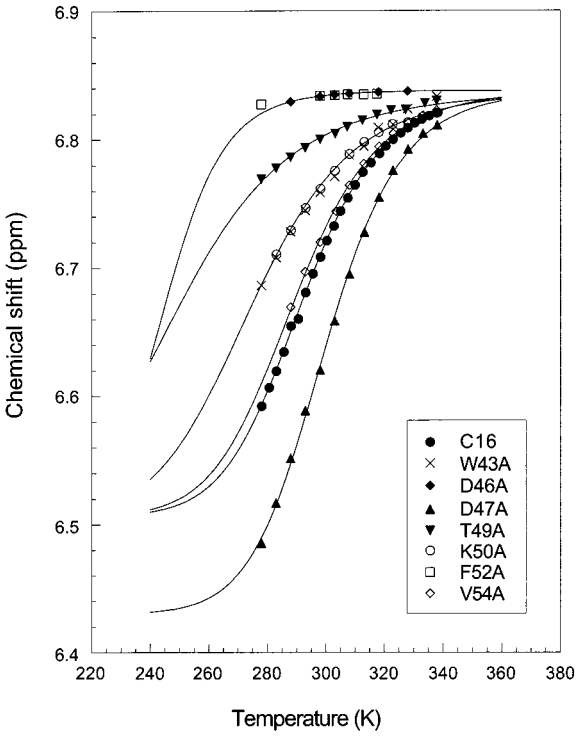

FIGURE 4: Chemical shift melting curves of the signals for C$^\epsilon$H-Tyr45 protons of seven mutants plotted against temperature from 278 to 338 K. Solid lines indicate the best-fitted theoretical curves calculated by eq 1.

ppb/K at 278−283 K. This chemical shift change is much larger than that of a random-coil peptide. In the case of several N-terminal fragments derived from the protein G B1 domain, it was less than 0.8 ppb/K (*28*). In Figure 4, the chemical shift values of the C$^\delta$H-Tyr45 signals of the PGB1-(41−56) mutants were plotted against temperature, where five of them, W43A, D47A, K50A, T49A, and V54A, showed large dependencies on temperature, while D46A and F52A were nearly independent. Similar to our recent work (*36*), the melting curves were studied by RT plot analysis and only one mutant D47A represented an obvious inflection point in their thermal transition. Then, the restricted nonlinear fitting calculation was carried out on the chemical shift melting curve of D47A using the eq 1. For this calculation, T_m value roughly estimated from the RT plot analysis was used as an initial value, and Y_F value was set to be a variable. In contrast, no distinctive inflection point was observed in the RT plot of D46A, T49A, and K50A, indicating the melting data of these mutants covered only a part of the broad transition, i.e., the transition temperature might be under the freezing point of the solvent. To converge the variable parameters in the fitting calculations, for a most reasonable approximation, Y_F values of these three mutants were set to be constant corresponding to the value of the wild-type. The obtained thermodynamic parameters are listed in Table 1. In comparison of their T_m and $\Delta\Delta G(298)$ values, the order of thermodynamic stability of the mutants is represented as D47A > wild-type ≈ V54A > K50A > T49A > D46A.

In the quantitative analysis, the mutants with the substitution for the aromatic side chains, W43A, Y45A, and F52A, were excluded, because we considered the substitution for the aromatic amino acid residue, i.e., removal of the strong ring current effect, might cause considerable change in the Y_F values. Nevertheless, it is remarkable that the substitution

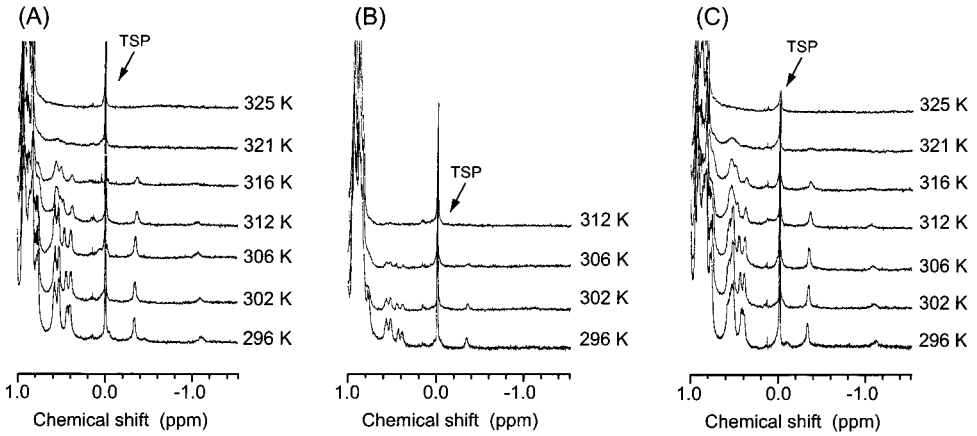

FIGURE 5: 1D ^{1}H NMR spectra for the equimolar mixture (0.5 mM) PGB1(1−40) + PGB1(41−56) (A), PGB1(1−40) + D46A (B), and PGB1(1−40)+D47A (C). The spectra of the mixtures were measured in 100% D_2O, containing 5 mM sodium phosphate buffer (pH 7.0) at varied temperature from 296 to 325 K.

Table 1: Thermodynamic Parameters for Unfolding of β-hairpin Structure of PGB1(41−56) Mutants Determined by Chemical Shift Melting Measurements of Nonpolar Side-Chain Signals[a]

mutant	T_m (K)	ΔH_m (kJ mol^{-1})	ΔS_m (J K^{-1} mol^{-1})	$\Delta\Delta G(298)$ (kJ mol^{-1})
wild-type[b]	293 ± 4.3[c]	53 ± 5.1	181 ± 18	
D47A	300 ± 1.8	60 ± 3.2	198 ± 10	1.5 ± 1.1
V54A	289 ± 0.4	49 ± 2.5	169 ± 8.8	−0.4 ± 0.9
K50A	277 ± 2.7	38 ± 2.3	138 ± 7.7	−1.9 ± 1.1
T49A	257 ± 7.7	29 ± 2.0	111 ± 6.0	−3.6 ± 1.5
D46A	252 ± 5.5	35 ± 11	139 ± 46	−5.7 ± 3.7
W43A		medium destabilization[d]		
Y45A		strong destabilization[d]		
F52A		strong destabilization[d]		

[a] Mean values are calculated from the analysis on C$^\epsilon$H-Trp43, C$^\delta$H-Tyr45, C$^\epsilon$H-Tyr45, and C$^\zeta$H-Phe52. For the mutants of V54A and D46A, the mean values are calculated from the analysis on C$^\epsilon$H-Trp43, C$^\delta$H-Tyr45 and C$^\epsilon$H-Tyr45, and C$^\epsilon$H-Trp43, C$^\delta$H-Tyr45, and C$^\zeta$H−Phe52, respectively. [b] Values for wild-type are from our previous report (*36*). [c] Deviations between the values evaluated from the signals. [d] Quantitative analysis for the three mutants W43A, Y45A, and F52A were not conducted. The reason is mentioned in the text.

of aromatic residues, especially in Y45A and F52A, dramatically reduced the temperature dependence (Figure 4), potentially suggesting the large contribution of the aromatic groups for the β-hairpin folding of PGB1(41−56). The α-proton and aliphatic signals of Y45A and F52A also showed less dependence of temperature (data not shown). Moreover, the sharp and crowded signals of the mutants at 298 K definitely feature a typical random coil state of a protein. Considering these results, it is concluded that the mutation on the residues Tyr45, Asp46, Thr49, and Phe52 is critical on the β-hairpin folding of PGB1(41−56).

Thermodynamic Stability of the Complex of PGB1(41−56) Mutants with PGB1(1−40). We measured 1D ^{1}H NMR spectra for the mixtures of PGB1(1−40) and the PGB1(41−56) mutants, to examine how the mutation on PGB1(41−56) will affect the specific interations in the complementary complex with PGB1(1−40). Figure 5 shows the spectra of equimolar mixtures of PGB1(1−40) with PGB1(41−56) wild-type, D46A or D47A measured at the temperature range from 296 to 325 K. The aliphatic and α-proton signals were largely shifted to upfield and downfield, respectively, while the aromatic signals were widely spread in the four complexes at 296 K (data not shown for K50A and T49A). The spectral features of the complexes with these mutants were very similar to that of the complex with the wild-type, indicating that all complexes can form a nativelike structure of the whole domain. In contrast, the spectra of the mixtures of PGB1(1−40) and aromatic mutant W43A, Y45A or F52A showed a lot of sharp and crowded signals (data not shown), indicating no interaction between the peptides, i e., no complex formation even at the lowest temperature, 296 K. The most probable explanation for the result is that the mutation of the aromatic residue removed a lot of native interactions in the hydrophobic core, resulting in a significant destabilization of the complex. The intensity of the signals in the upfield and downfield regions was decreased significantly as increasing temperature, but kept showing the same chemical shift. This indicates that the exchange rate between folded and unfolded states of the complexes were much slower than the NMR time scale under the condition of the present measurements [for the complex of wild-type pair, folded/unfolded exchange is coupled with associated/dissociated exchange (*36*−*38*)]. Therefore, the fraction of the folded complex was straightforwardly evaluated from the integrated value of the signals in the spectra. Figure 6 shows the intensity melting curves of the complexes that were obtained by monitoring the signal of C$^\gamma$H$_3$-Val54 highly shifted around −0.3 ppm. According to the fitting procedure based on the three component equilibrium system (AB ⇌ A + B) established in our previous report (*38*), the thermodynamic parameters characterizing the stability of the complexes were obtained (Table 2). In comparison of the T_m and $\Delta\Delta G(298)$ values, the order of thermodynamic stability of the complexes is represented as D47A > PGB1(41−56) (wild-type) > T49A > K50A > D46A ≫ W43A, Y45A, F52A. Interestingly, this stability order of the complexes was found to correlate well with the stability order of the mutants alone.

DISCUSSIONS

In this study, we have shown that most of the mutations on the side chains of aromatic residues and hydrophilic residues significantly reduced the thermal stability of the short C-terminal fragment, PGB1(41−56). Additionally, the influences of the mutations are not localized on a certain

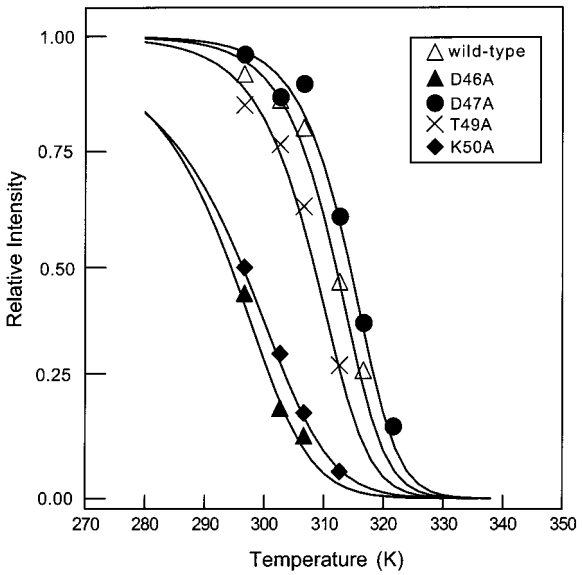

FIGURE 6: Intensity melting curves of the complexes of PGB1(1−40) with PGB1(41−56), D46A, D47A, T49A, and K50A, respectively. Vertical scale represents the relative intensity of $C^{\gamma}H_3$-Val54 signal in the complex form. Solid lines indicate the best-fitted theoretical curves calculated by eq 2 and 3.

Table 2: Thermodynamic Parameters for Unfolding of the Complex of PGB1(41−56) Mutants with PGB1(1−40) Determined by Intensity Melting Measurements[a]

mutant	T_m (K)	ΔH_m (kJ mol^{-1})	$\Delta\Delta G(298)$ (kJ mol^{-1})
wild-type	312 ± 1.0[b]	212 ± 26	
D47A	315 ± 0.8	201 ± 29	1.2 ± 0.2
T49A	309 ± 1.1	192 ± 7	−2.0 ± 0.9
V54A	303	154	−4.5
K50A	301 ± 0.8	156 ± 8	−7.0 ± 1.3
D46A	296 ± 2.1	154 ± 24	−9.5 ± 0.7
W43A		no complex[c]	
Y45A		no complex[c]	
F52A		no complex[c]	

[a] Mean values are shown from the analysis on the signals of $C^{\zeta}H$-Phe52 and $C^{\gamma}H$-Val54 except for the mutant V54A, showing only the values from the analysis on the signal of $C^{\zeta}H$-Phe52. [b] Deviations between the values calculated from the signals. [c] Quantitative analysis for the mixtures of three mutants W43A, Y45A, and F52A with PGB1(1−40) were not conducted because no detectable signal for the complex was observed.

region close to the mutation site. These results confirms the high cooperativity of the β-hairpin folding again, which would be hardly found in a short linear peptide.

Role of Nonpolar Side Chains. All the nonpolar residues mutated in this study are located on the β-strand in the whole domain structure. The side chains of Trp43 and Val54 are in contact each other in both NMR and crystal structure of whole domain as well as the side chains of Tyr45 and Phe52 (*21*−*24*). Furthermore, the clustered side chains, Trp43−Val54 are close enough (3−4 Å) to Tyr45−Phe52 to interact with their side chains. Nevertheless, our results showed that the influence of mutation of Val54 on the thermal stability of PGB1(41−56) was negligible compared with the others. Blanco et al. have shown several interstrand NOEs in the NMR study of PGB1(41−56) as the strong evidence for the formation of a nativelike β-hairpin structure, but no interstrand NOE between the side chain of Val54 and other residues (*29*). Therefore, it could be concluded that the side chain of Val54 contributes less in stabilizing the hydrophobic cluster of PGB1(41−56). Interestingly, this agrees with the recent simulation study on this peptide (*32*), in which only the side chain of Val54 was released from the hydrophobic cluster, but the other three aromatic side chains were retained in the earliest stages of unfolding process of PGB1(41−56). The chemical shift melting curves of the three aromatic mutants were not analyzed quantitatively, because we considered that the removal of the aromatic ring would affect the ring current distribution of the hydrophobic cluster, which could mislead chemical shift values of the mutants in the completely folded state. Although we did not quantitatively compare thermodynamic parameters for the three mutants W43A, Y45A, and F52A, the spectra of the latter two were nearly independent of temperature that is a typical feature of ideally unfolded proteins. These dramatic changes by the mutations of Tyr45 and Phe52 allow us to conclude that these two side chains contribute substantially in stabilizing the β-hairpin structure of PGB1(41−56). The influence of the mutation of Trp43 appears moderate compared with the other mutants. Thus, we could conclude at least that the contributions of the side chain of Trp43 are not more than that of Tyr45 and Phe52. In the Blanco's report (*29*), many interstrand NOEs were found between the side chains of Tyr45 and Phe52; however, only a few NOEs were observed from the side chains of Trp43 to the other nonpolar side chains. More recently, Dinner et al. have investigated free-energy surface of PGB1(41−56) by multicanonical Monte Carlo simulation (*33*). In the study, they have pointed out that a hydrophobic assembly stabilized by a strong interaction between the aromatic side chains of Tyr45 and Phe52 forms in early folding events. These findings in the previous reports are consistent with our results, which suggests that the hydrophobic cluster of PGB1(41−56) is composed of the three side chains of Trp43, Tyr45, and Phe52, and that the interaction between those of Tyr45 and Phe52 is predominant.

Role of Polar Residues in the Loop Region (*46*−*51*). In the three-dimensional structure of protein G (*21*−*24*), the six residues from Asp46 to Thr51 form a rigid loop structure, which is similar in conformation as found in crystal or solution structures. The loop region bends up toward outside of the protein and is exposed to solvent. A characteristic hydrogen bond network is found within the loop region, e.g., between the side chain of Asp46 and the main chain of Ala48 and between the side chain of Thr49 and the side chain of Thr51. Our quantitative analysis on the thermodynamic stability of the mutants showed that most of the mutations on the loop region largely destabilize the PGB1(41−56) with the exception of the mutation on Asp47. Interestingly, Frank et al. (*43*) have demonstrated the existence of residual structure in the β-hairpin region of urea denatured protein G B1 domain. They have emphasized that Asp46, Thr49, and Thr51 are conformationally restricted even in the denatured state of the protein, which is in agreement with our observations. Consequently, the most likely explanation for our results is that the side chains of Asp46, Thr49, and Lys50 have an important role in stabilizing the rigid loop region (46−51) by restricting rotational freedom of the main chains and/or the side chains with the characteristic hydrogen bond network.

Role of Residues in PGB1(41−56) for Complex Formation. From the results of the intensity-melting experiments using the complex of PGB1(41−56) mutants with PGB1-(1−40), we found that all the aromatic mutations seriously destabilize each complex. This observation indicates that hydrophobic interactions in the cluster of β-hairpin are crucial for the complex formation. Moreover, most of the mutations in the loop (46−52) also caused destabilization of the complex. The loop is significantly exposed to solvent in the intact domain, which means the residues in the loop might not interact with the other region of PGB1(41−56) strongly. Therefore, the destabilization by the mutations on the loop would be inferred as a result of increase in entropic term of rigid loop rather than by enthalpic one on the substituted residue. In other words, the difference in entropy from folded (associated) to unfolded (dissociated) states was reduced by the local restriction at the loop, which must be favorable for the stability of the complex. The entropic effect of β-hairpin structure upon folding of the domain has been also investigated in our previous study using the cyclized mutant with a disulfide bond (*39*). It is interesting to note that the stability order of the mutant alone is approximately the same as that of the complex. This indicates that several key residues in PGB1(41−56) are responsible for not only local interactions but also the global stability of the whole domain. Furthermore, the influence of the mutation on Asp46 is in sharp contrast to that on Asp47, suggesting that the conformationally favored local interactions in the loop region are quite important in the global stability of the whole domain.

Our mutagenesis study on the PGB1(41−56) suggests that the two factors are coexisting in the folding of PGB1(41−56): (i) the strong hydrophobic interactions between the side chains of the aromatic residues Tyr45 and Phe52 and (ii) the a rigid structure at the loop region (46−51). Cooperative work of these two factors bends this peptide itself and promote the hydrogen bonds between the two antiparallel strands. This would be the reason such a short linear peptide forms the stable structure under physiological conditions. From the present and relating works on the PGB1(41−56), the role of the side chains in the stability and the cooperative formation of the β-hairpin has been investigated extensively. Moreover, recent kinetic studies have revealed the very fast folding behavior of both the peptide alone (*31*) and the whole domain (*27*). However, it is still difficult to say whether the β-hairpin structure accumulates as a definitive intermediate or where it is involved in the folding nucleus of a transition state along the folding pathway of the whole domain. Nevertheless, our study strongly suggests that key residues in the hydrophobic cluster and the loop studied here play significant roles in stabilizing either an intermediate or a transition state in the folding process of protein G.

ACKNOWLEDGMENT

We thank Dr. Ishibashi and Ms. Yoshida, Takeda Chemical Industries Co. Ltd., for measurements of FAB mass spectroscopy. N.K. is supported by a fellowship of the Japan Society for the Promotion of Science. We also wish to thank Dr. Farid Khan for discussions of the manuscript.

REFERENCES

1. Wright, P. E., Dyson, H. J., and Lerner, R. A. (1988) *Biochemistry 27*, 7167−7175.
2. Shortle, D., and Meeker, A. K. (1989) *Biochemistry 28*, 936−944.
3. Kim, P. S., and Baldwin, R. L. (1990) *Annu. Rev. Biochem. 59*, 631−660.
4. Dyson, H. J., and Wright, P. E. (1991) *Annu. Rev. Biophys. Biophys. Chem. 20*, 519−538.
5. Dyson, H. J., Merutka, G., Waltho, J. P., Lerner, R. A., and Wright, P. E. (1992) *J. Mol. Biol. 226*, 795−817.
6. Dyson, H. J., Sayre, J. R., Merutka, G., Shin, H.-C., Lerner, R. A., and Wright, P. E. (1992) *J. Mol. Biol. 226*, 819−835.
7. Kuroda, Y. (1993) *Biochemistry 32*, 1219−1224.
8. Sancho, J., and Fersht, A. R. (1992) *J. Mol. Biol. 224*, 741−747.
9. Shin, H.-C., Merutka, G., Waltho, J. P., Wright, P. E., and Dyson, H. J. (1993) *Biochemistry 32*, 6348−6355.
10. Shin, H.-C., Merutka, G., Waltho, J. P., Tennant, L. L., Dyson, H. J., and Wright, P. E. (1993) *Biochemistry 32*, 6356−6364.
11. Kippen, A. D., Sancho, J., and Fersht, A. R. (1994) *Biochemistry 33*, 3778−3786.
12. Waltho, J. P., Feher, V. A., Merutka, G., Dyson, H. J., and Wright, P. E. (1993) *Biochemistry 32*, 6337−6347.
13. Kim, P. S., and Baldwin, R. L. (1982) *Annu. Rev. Biochem. 51*, 459−489.
14. Go, N. (1983) *Annu. Rev Biophys. Bioeng. 12*, 183−210.
15. Itzhaki, L. S., Otzen, D. E., and Fersht, A. R. (1995) *J. Mol. Biol. 254*, 260−288.
16. Panchenko, A. R., Luthey-Schulten, Z., and Wolynes, P. G. (1996) *Proc. Natl. Acad. Sci. U.S.A. 93*, 2008−2013.
17. Fahnestock, S. R., Alexander, P., Nagle, J., and Filpula, D. (1986) *J. Bacteriol. 167*, 870−880.
18. Sjöbring, U., Björck, L., and Kastern, W. (1991) *J. Biol. Chem. 266*, 399−405.
19. Olsson, A., Eliasson, M., Guss, B., Nilsson, B., Hellman, U., Lindberg, M., and Uhlén, M. (1987) *Eur. J. Biochem. 168*, 319−324.
20. Guss, B., Eliasson, M., Olsson, A., Uhlén, M., Frej, A. K., Jörnvall, H., Flock, J. I., and Lindberg, M. (1986) *EMBO J. 5*, 1567−1575.
21. Gronenborn, A. M., Filpula, D. R., Essig, N. Z., Achari, A., Whitlow, M., Wingfield, P. T., and Clore, G. M. (1991) *Science 253*, 657−661.
22. Lian, L.-Y., Derrick, J. P., Sutcliffe, M. J., Yang, J. C., and Roberts, G. C. K. (1992) *J. Mol. Biol. 228*, 1219−1234.
23. Achari, A., Hale, S. P., Howard, A. J., Clore, G. M., Gronenborn, A. M., Hardman, K. D., and Whitlow, M. (1992) *Biochemistry 31*, 10449−10457.
24. Gallagher, T., Alexander, P., Bryan, P., and Gilliland, G. L. (1994) *Biochemistry 33*, 4721−4729.
25. Alexander, P., Orban, J., and Bryan, P. (1992) *Biochemistry 31*, 7243−7248.
26. Alexander, P., Fahnestock, S., Lee, T., Orban, J., and Bryan, P. (1992) *Biochemistry 31*, 3597−3603.
27. Park, S.-H., Shastry, M. C. R., and Roder, H. (1999) *Nat. Struct. Biol. 6*, 943−947.
28. Kobayashi, N., Endo, S., and Munekata, E. (1993) *in Peptide Chem. 1992* (Yanaihara, N., Ed.) pp 278−280, ESCOM, Leiden, The Netherlands.
29. Blanco, F. J., Rivas, G., and Serrano, L. (1994) *Nat. Struct. Biol. 1*, 584−590.
30. Muñoz, V., Thompson, P. A., Hofrichter, J., and Eaton, W. A. (1997) *Nature 390*, 196−199.
31. Muñoz, V., Henry, E. R., Hofrichter, J., and Eaton, W. A. (1998) *Proc. Natl. Acad. Sci. U.S.A. 95*, 5872−5879.
32. Pande, V. S., and Rokhsar, D. S. (1999) *Proc. Natl. Acad. Sci. U.S.A. 96*, 9062−9067.
33. Dinner, A. R., Lazaridis, T., and Karplus, M. (1999) *Proc. Natl. Acad. Sci. U.S.A. 96*, 9068−9073.
34. Roder, H. (1989) *Methods Enzymol. 176*, 446−473.
35. Oas, T. G., and Kim, P. S. (1988) *Nature 336*, 42−48.
36. Honda, S., Kobayashi, N., and Munekata, E. (2000) *J. Mol. Biol. 295*, 269−278.

37. Kobayashi, N., Honda, S., Yoshii, H., Uedaira, H., and Munekata, E. (1995) *FEBS Lett. 366*, 99−103.
38. Honda, S., Kobayashi, N., Munekata, E., and Uedaira, H. (1999) *Biochemistry 38*, 1203−1213.
39. Kobayashi, N., Honda, S., and Munekata, E. (1999) *Biochemistry 38*, 3228−3234.
40. Gill, S. C., and von Hippel, P. H. (1989) *Anal. Biochem. 182*, 319−326.
41. Tomski, S. J., and Murphy, R. M. (1992) *Arch. Biochem. Biophys. 294*, 630−638.
42. Terzi, E., Hölzemann, G., and Seelig, J. (1995) *J. Mol. Biol. 252*, 633−642.
43. Frank, M. K., Clore, G. M., and Gronenborn, A. M. (1995) *Protein Sci. 4*, 2605−2615.
44. Kraulis, P. J. (1991) *J. Appl. Crystallogr. 24*, 946−950.

BI000013P